Michigan State University

National Superconducting Cyclotron Laboratory

PROTON HALOS IN THE 1s0d SHELL

B.A. BROWN and P.G. HANSEN

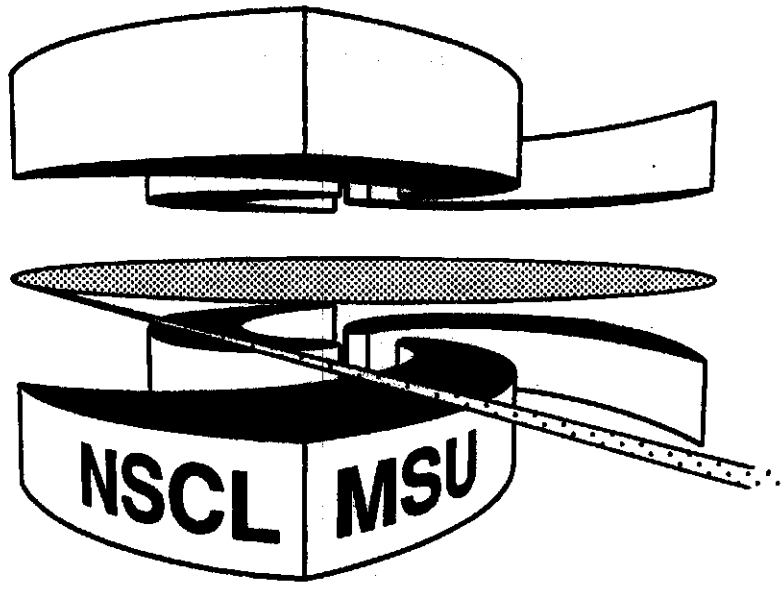

MSUCL-1023

APRIL 1996

Proton halos in the 1s0d shell

B. A. Brown and P. G. Hansen

Department of Physics and Astronomy and National Superconducting *Cyclotron Laboratory,*

Michigan *State University, East* Lansing, Michigan *48824*

Abstract

The shell-model properties of proton halo states in proton-rich 1s0d shell nuclei are investigated. The most interesting cases appear to be those in ^{26,27}P and ^{27}S. The parallel-momentum distributions of core fragments from proton stripping reactions may provide experimental insight into the structure of the halo states and the role played by the reaction mechanism. The "generalized Coulomb shift", defined as the difference between the proton separation for the proton-rich nucleus and the neutron separation energy for the analogue neutron-rich nucleus, is shown to be nearly constant and provides a good tool for proton-rich mass extrapolations. The relation between the total interaction cross section and the matter radius is discussed.

Nuclei near the proton and neutron drip lines often have matter distributions which extend to large radii due to the loose binding of the last one or two nucleons. The extended distributions are referred to as "halos". [1,2] The halo has been observed experimentally from an increase of the total reaction cross section, which is related to the total matter density, and from momentum distribution in break-up reactions, which is related to the density of the valence orbital. One of the simplest ground-state examples is "Be where the last neutron is predominantly in a $1s_{1/2}$ state [3] and is bound only by 0.50 MeV. The density distribution of the valence neutron is extended with an rms radius [2,4,5] of about 6.0 fm, and the parallel-momentum distribution in the reaction (^{11}Be,^{10}Be) is correspondingly

narrow, [6] 42±2 MeV/c for a light target, due of the loose binding, and because there is no centrifugal or Coulomb barrier. There is a similar case which has been recently studied [7,8] in ^{19}C. Other examples [1,2,5] on the neutron-rich side are the loosely bound di-neutron systems such as ^{11}Li and ^{14}Be.

The analogues of the cases mentioned above on the proton-rich side are all unbound. Perhaps the simplest example of a bound-state proton halo is that of the $1/2^+$ first excited state of ^{17}F which is bound by 0.10 MeV. This state is described in zeroth order by a $1s_{1/2}$ configuration outside of an ^{16}O closed shell, and has a calculated [9] rms valence radius of 5.5 fm. However, since this is an excited state its reaction cross section and momentum distribution cannot be studied, and its proton halo nature is inferred from the large Thomas-Ehrman Coulomb shift relative to the $5/2^+$ T=1/2 ($0d_{5/2}$) ground state [10,11] and from the large $1/2^+$ to $5/2^+$ B(E2) value. [9] In general, for a fixed angular momentum and fixed separation energy, the size of the proton halo states are not as large as the neutron halo states because of the Coulomb barrier.

The only case on the proton-rich side whose break-up distribution of parallel momentum[1] has been studied is that of ^{8}B. The valence proton in this case is bound by 0.137 MeV and the calculated [12] valence $0p$ proton rms radius is 4.4 fm. Its measured momentum distribution [13,14] is, however, almost a factor of two narrower than that predicted from the Fourier transform of the spatial wave function of the valence nucleon, and this is presumably [12,15] related to the fact that the proton stripping reaction only samples the valence density beyond a minimum impact parameter b_{min}. This can be defined as the sum of the

---

[1] In the present paper we restrict the discussion of momentum distributions to the parallel momentum measured in reactions such as (^{26}P,^{25}Si) etc. on light targets because this parameter seems particularly simple to interpret. It should be clear that valuable additional characterization of halo states can be obtained from the transverse momentum components and from Coulomb excitation of the halo.

(experimentally determined) energy-dependent interaction radii of the core fragment and the target. For ^{8}B incident at 1.47 GeV/u on a carbon target one has a b_{min} of 4.8 fm. An estimate based on an eikonal picture can account both for the momentum content of the halo wave function and for the absolute cross section, which can be linked to that for free nucleons of the same velocity. The effects of the localization of the reaction to the external part of the wave function are strongly dependent on the separation energy of the halo nucleon and its angular momentum. In the case of a neutron in an s state with parameters corresponding to those of ^{11}Be, the momentum width is rather close to that of the wave function as a whole, which is probably why the localization effect was not considered in early discussions of the parallel-momentum distributions.

The main thing missing from the cases discussed above is a good example of a proton-rich ground state whose structure is that of a valence proton $s_{1/2}$ orbital coupled to the ground state of the core. The natural place to look for such a configuration is in the middle of the $1s0d$ shell at the nuclei with Z=15 and Z=16, where in the simplest shell-model picture the $1s_{1/2}$ orbital becomes filled. An example is ^{29}P which is well known [16] to have a zeroth-order structure of a $1s_{1/2}$ proton outside a ^{28}Si closed shell, but its structure is not as simple as that of ^{17}F, and the full-$1s0d$ shell configuration mixing is needed [16,17] in order to explain the magnetic properties of ^{29}P and its mirror ^{29}Si. It is interesting to examine the properties of the more proton-rich isotopes of phosphorus (Z=15).

The one-proton separation energies, S_p, for the Z=15 isotopes [18] as a function of neutron number N are given in Table I. These are compared with the one-neutron separation energies, S_n, for N=15 as a function of proton number. The difference $\Delta_{pn} = S_p - S_n$, is also given. It clear that ^{26}P is potentially the most most interesting loosely bound case, as has been pointed out recently on the basis of relativistic mean-field calculations, [19] and it is known [20] to be particle-stable. The value of S_p has been derived [18] from systematic extrapolations, and the large error bars assigned to it and to some of the other cases by Audi and Wapstra [18] are only of symbolic significance.

The quantity Δ_{pn} is the generalized Coulomb shift. It can be modeled by calculating

the proton and neutron single-particle energies in a Woods-Saxon potential which has a Coulomb potential plus a common central potential for protons and neutrons. By varying the depth and/or radius of the central potential one can calculate the relationship between S_p and Δ_{pn}. The results for a typical Woods-Saxon potential are shown in Fig. 1. The solid line is the result obtained by varying the well depth for a fixed radius (R = 3.89 fm) and diffuseness (a = 0.65 fm), and the dashed line is the result obtained by varying the radius for a fixed well depth and diffuseness. The main point is that the calculated dependence of Δ_{pn} upon S_p is very smooth even very close to the proton threshold (when S_p goes to zero). This is because of the relatively large Coulomb barrier. The experimental values show a similar behavior. Taking into account this smooth behaviour, the S_p value for ^{26}P should be close to the Audi-Wapstra extrapolation of 0.14 MeV, and its uncertainty must be nearly an order of magnitude smaller than their estimated value of 0.20 MeV. (The overall shift between the experimental and theoretical values is related to the Nolen-Schiffer anomaly and as well as the various exchange-interaction and relativistic corrections which are left out of the calculation. [10])

The slope for the $1s_{1/2}$ state seen in Fig. 1 is related to the Thomas-Ehrman shift for the $1s_{1/2}$ halo state. It is interesting to compare these results for the $1s_{1/2}$ configuration to those for the isotopes with Z=13 and Z=14 which should be dominated by a $0d_{5/2}$ valence configuration, see Fig. 1. In this case the experimental values for Δ_{pn} are essentially flat as a function of S_p, and this is reproduced by the calculation for the $0d_{5/2}$ in which the radius is varied (the dashed line). The calculated curve for $0d_{5/2}$ shows a smaller slope relative to $0s_{1/2}$ due to the centrifugal barrier for ℓ=2.

The case of ^{26}P is more complicated than the usual one-nucleon halos because it has an odd number of both neutrons and protons. The properties of the mirror nucleus, ^{26}Na, obtained from β decay experiments [21,22] and from the USD [23] and SDPOTA [24] $1s0d$ shell-model interactions are summarized in Table II. Qualitatively, the low-lying quartet can be understood from the coupling of the odd $1s_{1/2}$ neutron to the $5/2^+$ ground state and $3/2^+$ low-lying (0.090 MeV) excited state in ^{25}Na. The order of the levels in the quartet is very

sensitive to the interaction with the SDPOTA interaction obtaining the correct assignment of 3^+ for the ground state. The two low-lying 1^+ states reported in Ref 21 from the beta decay of ^{26}Ne are inconsistent with the calculations. The 1^+ assignment to the 0.082 MeV state seems firm since it is very strongly fed in the ^{26}Ne β decay. [22] However, the state at 0.234 MeV is much more weekly fed [22] and it may be a 2^+ state fed from the predicted β decay to higher lying 1^+ states. [25]

Thus, the most likely spin for the ground state of the mirror nucleus ^{26}P is 3^+. In the full $0d1s$ shell-model calculation its main parentage is to the $5/2^+$ ground state of ^{25}Si with a $1s_{1/2}$ spectroscopic factor of $C^2S = 0.66$ (to be compared with $C^2S = 1.0$ in the zeroth-order shell model). The $0d_{5/2}$ spectroscopic factor is very small (0.002). The total proton occupation of the $1s_{1/2}$ orbital is 1.05 and the remaining 0.39 of the $1s_{1/2}$ spectroscopic strength goes to highly excited $5/2^+$ and $7/2^+$ states in ^{25}Si.

The halo structure of ^{26}P should thus be calculated as if it were 0.66 of $1s_{1/2}$ proton bound by about 0.14 MeV to the ^{25}Si ground state. In a typical Woods-Saxon geometry (the same one used in the discussion above), the rms radius of the $1s_{1/2}$ state is 4.71 fm. This can be compared to the total proton and neutron rms radius of the ^{25}Si core of 3.35 fm and 2.86 fm, respectively, see Fig. 2.

The behavior of the single-particle proton wave functions at large distances is dominated by the Coulomb barrier and the sensitivity to the proton separation energy is not large. This can be seen from the comparison of the radial densities for ^{26,27,28}P shown in Fig. 2, and which correspond to rms radii of 4.71, 4.37 and 4.11 fm, respectively. For comparison a corresponding $1s$ state neutron with an S_n of 0.14 MeV would have a radius of about 10.8 fm.

Not surprisingly, the calculated parallel-momentum distributions shown in Fig. 3 mirror closely the behavior of the spatial wave functions. The approximation used here for calculating the localization effect replaces the wave function in the tube swept by the target nucleus by its values along the axis defined by the impact parameter, the minimum of which is 6.2 fm for the case of a ^{9}Be target. Due to the strong effect of the Coulomb barrier, which

makes the external wave function fall off more rapidly, this approximation is less accurate than previous estimates [15] for lighter systems. It should give reasonable values for the momentum distributions but will underestimate the cross sections. For an assumed beam energy of 60 MeV/u and for phosphorus isotopes with masses 26, 27 and 28, the calculated localized widths are 58 (74), 66 (84) and 75 (94) MeV/c, respectively, for the full width at half maximum. The values in parentheses are those calculated for the total wave function. The corresponding calculated cross sections (assuming $C^2S = 1$) are 51, 35 and 22 mb, respectively, very similar to those of single-nucleon knock-out reactions on systems with normal binding.

It is feasible and should be very interesting to study the parallel momentum distributions experimentally. The best illustration [12,15] of the localization effect so far, that of the ^{8}B 0p state, has a single lobe in the wave function and the effect shows up as a narrowing of the observed distribution. In contrast to this, the absence in the phosphorus isotopes of the large momentum components corresponding to the inner lobe of the 1s state will provide another experimental signature for the contribution from the reaction mechanism.

It is also interesting to investigate the proton-halo aspects of the Z=16 isotopes. The one-proton separation energies are summarized in Table I and Fig. 1. It would appear from the Audi-Wapstra mass systematics that ^{26}S could be a loosely bound system, and this would be particularly interesting since the corresponding daughter nucleus ^{25}P is itself unbound. However, from the Δ_{pn} systematics it is clear that Δ_{pn} should be close to 6.0 MeV which when combined with S_n for ^{26}Na would make ^{26}S unbound by 0.42(7) MeV. In addition, ^{26}S is unbound to two-proton emission (see Table III). ^{27}S has a separation energy of 0.75 MeV. The properties of the $1s_{1/2}$ halo in ^{27}S should be very similar to that of ^{27}P shown in Figs. 2 and 3, since the one-proton separation energy is about the same in both cases. As pointed out in Ref 19, ^{27}S also has the property of a relatively loosely bound di-proton system. The two-proton separation energies for Z=16 (the sum of the single-nucleon separation energies for Z=15 and Z=16 in Table I) are given in Table III. It would be very interesting to try to apply the three-body techniques which have been used for ^{11}Li to the case of ^{27}S.

Finally, we note the case of ^{22}Si which is known [26] to be particle-stable but which has (see Table III) a small two-proton separation energy. Since the valence orbital is $0d_{5/2}$ it has essentially no halo. We have used the SGII Skyrme interaction [27] to carry out Hartree-Fock calculations for the proton and neutron densities of light nuclei. [5,28] (HF calculations for the $1s_{1/2}$ proton halos discussed above are indistinguishable from the Woods-Saxon calculations discussed, as long as the proton separation energy is fixed at the experimental value.) The results of such calculations for the rms matter radii of ^{22}Si and ^{22}O are 3.08 fm and 3.00 fm, respectively. Thus even though the $0d_{5/2}$ is loosely bound in ^{22}Si, the rms matter radius is only 2.5 percent larger; again this is due to the ℓ=2 centrifugal barrier and the Coulomb barrier. Although this case has not yet been studied, the total interaction cross sections for a similar pair of nuclei, ^{20}Mg and ^{20}O has recently been reported. [29] The Glauber model has been used to interpret the observed 7 percent increase in the ^{20}Mg cross section relative to ^{20}O as being related to a 6–8 percent increase in the rms matter radius. However, as above, the calculated rms matter radii for ^{20}Mg and ^{20}O are more nearly equal; 2.85 fm and 2.80 fm respectively. It has also been noted [30] that the A=20 Coulomb shifts are not consistent with a halo and that perhaps an exotic "tetra-proton" structure is needed to explain the radius change. However, the relationship between the matter radii and the total interaction cross sections may not be a simple as that given by the standard Glauber model interpretation, especially for nuclei near the drip lines. We note that ^{20}Mg with a proton separation energy of 2.65 MeV has only one bound excited state (a 2^+ state at about 1.7 MeV) as compared to ^{20}O with a neutron separation energy of 7.61 MeV which has many bound states. Thus the part of the total interaction cross section leading to states between 3 and 8 MeV in excitation energy will be part of the measured reaction cross section for ^{20}Mg, but will not contribute for ^{20}O, since the nucleus decays back to the ground state and is detected as ^{20}O. The size of this effect should be calculated or measured.

ACKNOWLEDGMENTS

This research was partly supported by the National Science Foundation grants PHY-94-03666 and PHY-95-28844.

References

1. A. C. Mueller and B. M. Sherrill, Annu. Rev. Nucl. Part. Sci. 43, 529 (1993).
2. P. G. Hansen, A. S. Jensen and B. Jonson, Annu. Rev. Nucl. Part. Sci. 45, 591 (1995).
3. H. Sagawa, B. A. Brown and H. Esbensen, Phys. Lett. B309, 1 (1993); T. Otsuka, N. Fukunishi and H. Sagawa, Phys. Rev. Lett. 79, 1385 (1993); H. Esbensen, B. A. Brown and H. Sagawa, Phys. Rev. C51, 1274 (1995).
4. D. J. Millener, J. W. Olness, E. K. Warburton and S. S. Hanna, Phys. Rev. C28, 497 (1983).
5. G. F. Bertsch, B. A. Brown and H. Sagawa, Phys. Rev. C39, 1154 (1989).
6. J. H. Kelley et al., Phys. Rev. Lett. 74, 30 (1995).
7. D. Bazin et al., Phys. Rev. Lett. 74, 3569 (1995).
8. F. M. Marques et al., IPC CAEN preprint LPCC 96-05.
9. B. A. Brown, A. Arima and J. B. McGrory, Nucl. Phys. A277, 77 (1977).
10. J. Nolen and J. P. Schiffer, Annu. Rev. Nucl. Sci. 19, 471 (1969).
11. R. Sherr and G. Bertsch, Phys. Rev. C32, 1809 (1985).
12. B. A. Brown, A. Csoto and R. Sherr, Nucl. Phys. A597, 66 (1996).
13. W. Schwab et al., Z. Phys. A350, 283 (1995).
14. J. H. Kelley et al., Bull. Am. Phys. Soc. 40, 978 (1995).
15. P. G. Hansen, Proceedings of the International Conference on Exotic Nuclei and Atomic Masses Conference, Arles 1995, edited by M. de Saint Simon and O. Sorlin, (Editions Frontieres) in press, and to be published.
16. B. A. Brown, Nucl. Phys. A522, 221c (1991).
17. B. A. Brown, R. Radhi and B. H. Wildenthal, Phys. Lett. 133B, 5 (1983).
18. G. Audi and A. H. Wapstra, Nucl. Phys. A595, 409 (1995).
19. Z. Ren, B. Chen, Z. Ma and G. Xu, Phys. Rev. C53, R572 (1996).
20. M. D. Cable et al., Phys. Rev. C30, 1276 (1984).
21. P. M. Endt, Nucl. Phys. A521, 1 (1990).

22. J. P. Dufour, private communication.

23. B. A. Brown and B. H. Wildenthal, Annu. Rev. Nucl. Sci. 38, 29 (1988).

24. B. A. Brown, W. A. Richter, R. E. Julies and B. H. Wildenthal, Ann. Phys. 182, 191 (1988).

25. B. H. Wildenthal, M. S. Curtin and B. A. Brown, Phys. Rev. C28, 1343 (1983).

26. M. G. Saint-Laurent et al., Phys. Rev. Lett. 59, 33 (1987).

27. N. van Giai and H. Sagawa, Nucl. Phys. A371, 1 (1981), N. van Giai and H. Sagawa, Phys. Lett. B106, 379 (1981)

28. B. A. Brown and W. A. Richter, unpublished.

29. L. Chulkov et al., GSI preprint 95-75 (1995).

30. L. Chulkov, E. Roeckl and G. Kraus, Z. Phys. A353, 351 (1996).

Figure captions:

Fig. 1: Δ_{pn} vs S_p. The experimental results [18] for Z=13 and Z=15 are given by the filled circles. The experimental results for Z=14 and Z=16 multiplied by (13/14) and (15/16), respectively, are given by crosses. The solid and dashed lines for Z=13,14 are the $0d_{5/2}$ calculations discussed in the text. The solid and dashed lines for Z=15,16 are the $1s_{1/2}$ calculations discussed in the text.

Fig. 2: The radial density probability distribution of the core and of the valence proton, the latter calculated in a single particle Woods-Saxon model for ^{26,27,28}P with proton separation energies assumed to be 0.14, 0.90 and 2.07 MeV, respectively. The valence proton distribution is normalized to unity.

Fig. 3: The parallel-momentum distributions calculated for the ^{26,27,28}P proton halos with parameters as in Table I and Fig. 2. The curves for mass 26 are those most to the left. The dashed curves represent the result for the total wave function. The full-drawn curves take into account that the interaction with the target (taken to be ^{9}Be) localizes the observation to distances beyond the minimum impact parameter. Note that in the latter case the complete disappearance of the plateau around 100-150 MeV/c representing the inner lobe of the spatial wave functions (Fig. 2).

TABLES

TABLE I. Proton separation energies for isotopes with proton number Z and the neutron separation energies for the mirror nuclei with N=Z. The numbers in square brackets are based upon the Audi and Wapstra mass systematics.

Z	N	nucleus	S_p	mirror nucleus	S_n	$\Delta_{pn} = S_p - S_n$
13	12	^{25}Al	2.271	^{25}Mg	7.331	5.059
	11	^{24}Al	1.871(4)	^{24}Na	6.959	5.088(4)
	10	^{23}Al	0.125(25)	^{23}Ne	5.201	5.075(25)
	9	^{22}Al	[0.02(9)]	^{22}F	5.230(13)	[5.21(10)]
	8	^{21}Al	[-1.26(30)]	^{21}O	3.807(12)	[5.07(30)]
14	13	^{27}Si	7.463	^{27}Al	13.058	5.595
	12	^{26}Si	5.518(3)	^{26}Mg	11.093	5.575(3)
	11	^{25}Si	3.509(11)	^{25}Na	9.011	5.602(11)
	10	^{24}Si	3.301(32)	^{24}Ne	8.865(10)	5.564(33)
	9	^{23}Si	[1.70(22)]	^{23}F	7.54(8)	[5.84(23)]
	8	^{22}Si	[1.24(36)]	^{23}O	6.85(6)	[5.60(36)]
15	14	^{29}P	2.748	^{29}Si	8.473	5.725
	13	^{28}P	2.066(4)	^{28}Al	7.725	5.660(4)
	12	^{27}P	0.897(35)	^{27}Mg	6.443	5.546(35)
	11	^{26}P	[0.14(20)]	^{26}Ne	5.616(14)	[5.47(20)]
	10	^{25}P	[-0.83(20)]	^{25}F	4.182(46)	[5.01(20)]
	9	^{24}P	[-0.8(5)]	^{24}O	3.86(10)	[4.8(5)]
16	15	^{31}S	6.133	^{31}P	12.311	6.178
	14	^{30}S	4.400(3)	^{30}Si	10.609	6.209(3)
	13	^{29}S	3.287(50)	^{29}Al	9.436	6.149(50)
	12	^{28}S	[2.46(16)]	^{28}Mg	8.504(2)	[6.04(16)]
	11	^{27}S	[0.75(28)]	^{27}Na	6.750(41)	[5.99(29)]

10	^{26}S	[0.19(36)]	^{26}Na	5.582(71)	[5.39(36)]

TABLE II. Low-lying states in ^{26}Na

	Experiment		USD		SDPOTA
J^π	Ex(MeV)	J^π	Ex(MeV)	J^π	Ex(MeV)
2^+	0.	1^+	0.	3^+	0.
1^+	0.082	3^+	0.182	2^+	0.034
1^+	0.234	2^+	0.187	1^+	0.273
	0.420	2^+	0.413	2^+	0.375

TABLE III. Two-proton separation energies for isotopes with proton number Z and the Two-neutron separation energies for the mirror nuclei with N=Z. The numbers in square brackets are based upon the Audi and Wapstra mass systematics.

Z	N	nucleus	S_{2p}	mirror nucleus	S_{2n}	$\Delta_{pn} = S_{2p} - S_{2n}$
14	13	^{27}Si	13.770	^{27}Al	24.424	10.654
	12	^{26}Si	7.789(3)	^{26}Mg	18.424	10.634(3)
	11	^{25}Si	5.280(10)	^{25}Na	15.971	10.691(10)
	10	^{24}Si	3.426(20)	^{24}Ne	14.066(10)	10.639(22)
	9	^{23}Si	[1.72(20)]	^{23}F	12.766(80)	[11.05(21)]
	8	^{22}Si	[-0.02(20)]	^{22}O	10.655(57)	[10.67(21)]
16	15	^{31}S	11.728	^{31}P	23.632	11.904
	14	^{30}S	7.148(3)	^{30}Si	19.083	11.935(3)
	13	^{29}S	5.352(50)	^{29}Al	17.161	11.809(50)
	12	^{28}S	[3.36(16)]	^{28}Mg	14.947(2)	[11.59(16)]
	11	^{27}S	[0.90(20)]	^{27}Na	12.366(38)	[11.47(21)]
	10	^{26}S	[-0.64(30)]	^{26}Na	9.765(56)	[10.40(30)]

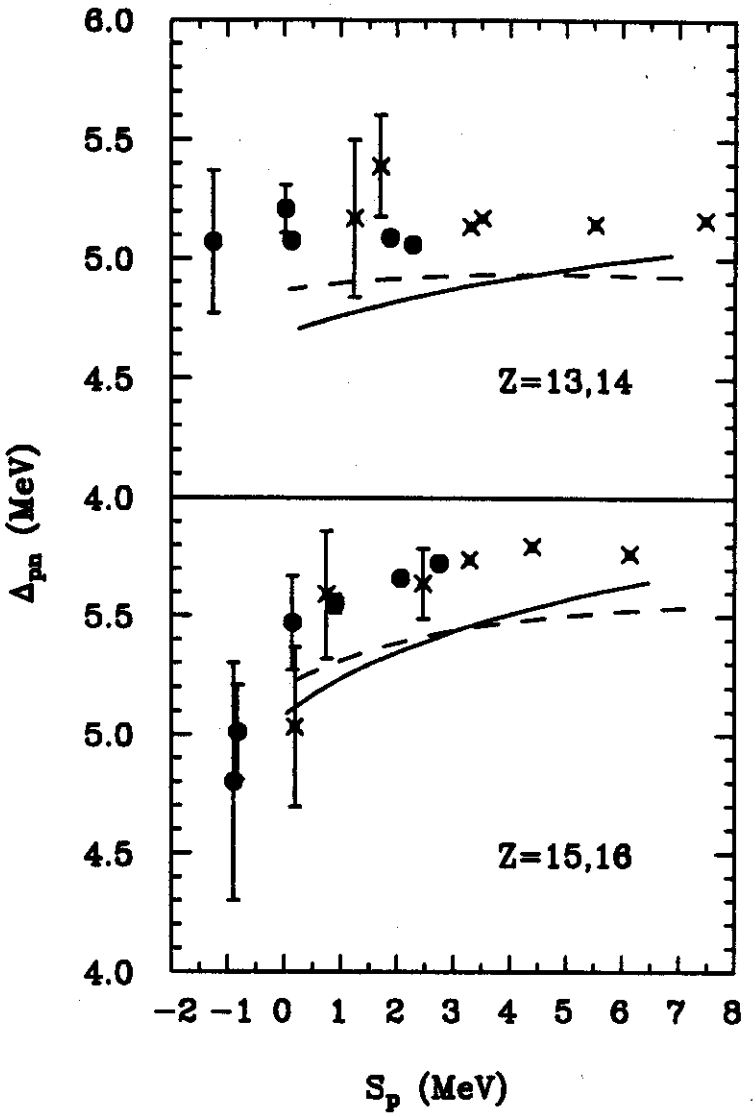

FIGURE 1

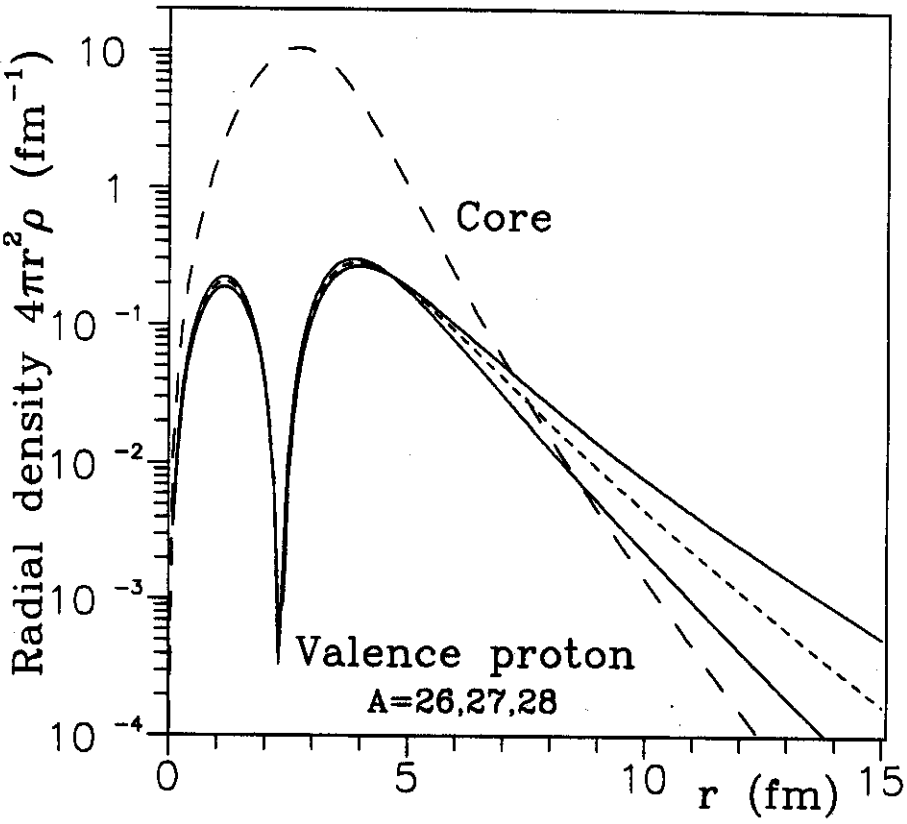
Radial density $4\pi r^2\rho$ (fm^{-1})
10
1
10^{-1}
10^{-2}
10^{-3}
10^{-4}
Core
Valence proton
A=26,27,28
0
5
10
15
r (fm)

FIGURE 2

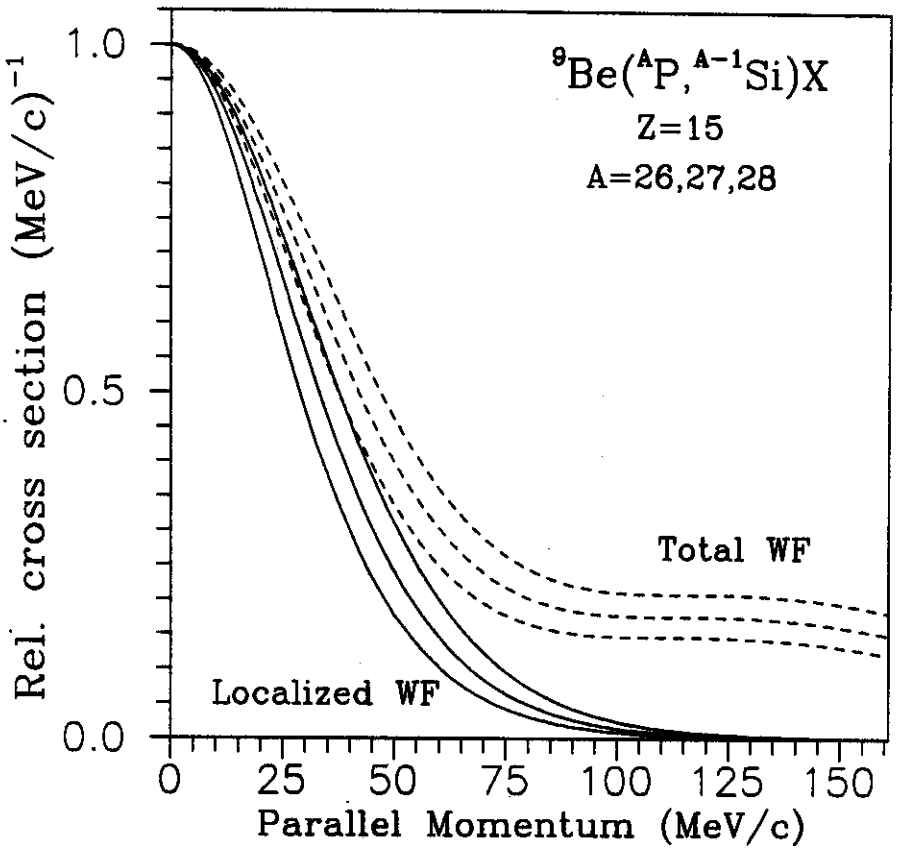
$^{9}Be(^{A}P,^{A-1}Si)X$
Z=15
A=26,27,28
Total WF
Localized WF
Rel. cross section (MeV/c)$^{-1}$
1.0
0.5
0.0
0
25
50
75
100
125
150
Parallel Momentum (MeV/c)

FIGURE 3